The Mandelbrot Set as a Modular Form

Linas Vepstas <linas@linas.org>

2 January 2005 (revised 30 May 2005)

Abstract

An exploration of the interior or the Mandelbrot Set and the appearance of functions appearing to be similar to modular forms. This provides yet another example of the close interconnection between the structure of the Modular Group SL(2,Z) and fractals. The relationship is demonstrated computationally and visually, and not from first principles; visually, the interior resembles the Weierstrass elliptic invariant g_2. However, it is a resemblance only; the various explicit expressions that can be found are shown to not actually be modular forms. It is hypothesized that some simple but currently unknown transformation will convert them into modular forms.

The construction of the interior is based on averaging together iterated values with a spectral-type summation, and then analyzing the asymptotic behavior of the sum. Leading divergence are easy to explain and remove; the remaining finite parts hint at modular symmetry.

This is a work in progress. A final conclusion and analysis has not been reached.

This paper is part of a set of chapters that explore the relationship between the real numbers, the modular group, and fractals. Updated and revised versions of this monograph can be found at `http://www.linas.org/math/sl2z.html`

1 Dedekind Eta and the Mandelbrot Set

XXX This paper may be subject to occasional revision. XXX

Modular forms are a particular kind of function on the complex upper half-plane studied in analytic number theory and the theory of elliptic curves. A precise definition of a modular form[**?**] will be given later in this paper. As a simple example, consider the Euler function

$$\phi(q) = \prod_{k=1}^{\infty}(1-q^k) \tag{1}$$

on the complex plane. It is closely related to the Dedekind eta function, which is a modular form. Figure 1 shows $\phi(q)$ inside the unit disk $|q| < 1$. Graphs of most modular forms visually resemble this picture in one way or another. The exploration presented in this monograph will be mostly visual, not algebraic; none-the-less, various basic expressions will be developed to make the hypothesis as explicit as possible.

Figure 1: Euler Function

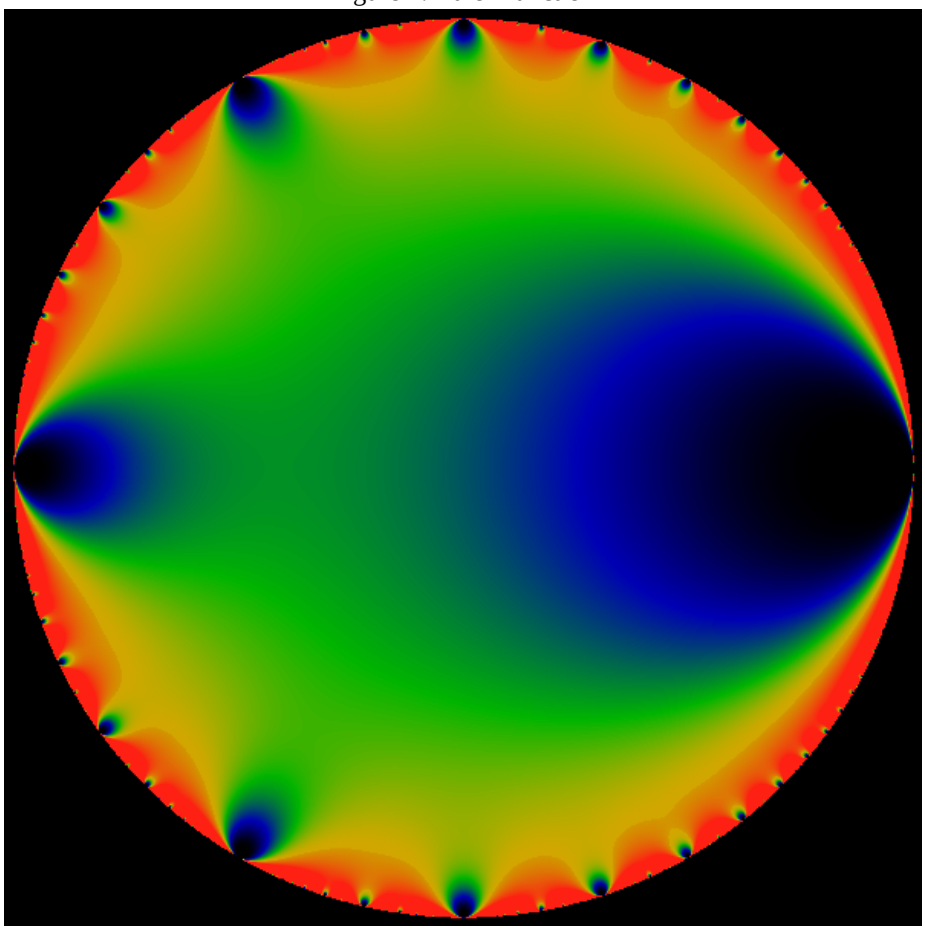

A rendition of the absolute value $|\phi(q)|$ of the Euler function on the q-disk. Note the readily apparent fractal self-similarity. This type of self-similarity is explicitly associated with the properties of the modular group $PSL(2,\mathbb{Z})$. A crude general resemblance to the structure of the Mandelbrot set should be equally evident. This paper is devoted to making this vague resemblance into a relationship as concrete as possible.

Now consider the Mandelbrot set. By means of a sequence of figures below, we shall uncover a structure inside the Mandelbrot set that appears to be some kind of modular form. The general development will be as follows: the first section develops a set of series that capture the asymptotic behavior of an iterated function. In the next section, these series are then applied to the Mandelbrot set iterator, where they are found to contain divergent and finite terms. The next section develops explicit, exact expressions for the divergent terms. The remainder of the paper is devoted to an exploration of the finite terms, and attempts to draw analogies to such modular forms as the Weierstrass elliptic invariant g_2 and to series involving the divisor function. Both the main cardioid and the large western bulb are explored. The paper concludes with an appendix reviewing the numeric techniques of series acceleration.

This paper is an expansion and revision of an earlier paper posted at `http://www.linas.org/art-gallery/spectral/spectral.html`.

1.1 Regulated Series

This section reviews the construction of a regulated series. These series will be used to perform a kind of averaging over the values of an iterated function; the asymptotic behavior of an iterated function may be studied in terms of these series.

Consider the sequence $\{a_0, a_1, a_2, ...\}$. Then for small positive t, construct the sum

$$S(t) = \sum_{n=0}^{\infty} a_n e^{-tn} \tag{2}$$

In the following,we'll refer to this as the *regulated series for the sequence* $\{a_n\}$. For large class of reasonably behaved series $\{a_n\}$, this sum is finite for all positive values of t. By 'reasonably behaved' we mean a sequence where a_n doesn't get exponentially large with increasing n; that is, one where the sum converges.

This sum participates in some interesting number-theoretic relationships when the $\{a_n\}$ are considered to be the spectrum of an operator. In the following, we will be considering the $\{a_n\}$ not as a spectrum, but instead as the iterates of the Mandelbrot Set. Before doing so, lets quickly review some basic properties.

One can define a Dirichlet series

$$C(s) = \sum_{n=0}^{\infty} \frac{a_n}{n^s} \tag{3}$$

which can be easily converted into the first sum with an integral transform.

The spectral analysis consists of exploring the behavior of the sum in the limit of $t \to 0$. Depending on the series, it may diverge. For example, if we take all a_n to be one, the sum $N(t) = \sum_{n=0}^{\infty} \exp(-tn)$ diverges as 1/t, while $\sum_{n=0}^{\infty} n \exp(-tn)$ diverges as $1/t^2$. The corresponding Dirichlet series exhibit poles at $s = 1$ and $s = 2$, respectively, for these sums. The core idea behind spectral analysis is that in general, one can gain insight into the structure of the series $\{a_n\}$by understanding the analytic structure of the related series. In other words, instead of studying $\{a_n\}$ directly, we study the expansion

$$S(t) = \sum_{n=-N}^{\infty} s_n t^n \tag{4}$$

instead.

When engaging in numerical calculations, the Dirichlet series is nearly numerically intractable, because of its painfully slow convergence. Thus,one is instantly motivated to use the exponential series instead. However, one gets an even more stable and numerically well-behaved series by considering the Gaussian regulator, namely

$$\sum_{n=0}^{\infty} a_n \exp(-t^2 n^2) \tag{5}$$

There is no harm in using this series for numerical work; it can be related back to the Dirichlet series through analytic integral transforms, albeit somewhat more complex ones than the plain exponential series. This, and some numerical subtleties, are discussed in a later section.

1.2 The Spectral Analysis of the Mandelbrot Set

Now consider the standard Mandelbrot set iteration

$$z_{n+1} = z_n^2 + c \tag{6}$$

ant the regulated series for this sequence of points

$$S_c(t) = \sum_{n=0}^{\infty} z_n e^{-t^2 n^2} \tag{7}$$

where we've added the subscript c to remind us that this series takes on distinct values for every point $c \in \mathbb{C}$. For most of the interior of the Mandelbrot set, this sum diverges as $1/t$. To normalize this sum, let us define

$$N(t) = \sum_{n=0}^{\infty} e^{-t^2 n^2} \tag{8}$$

which also diverges as $1/t$. Figure 2 shows the nature of the divergence by normalizing against this value. As a practical matter when performing numerical computations, it is more appropriate to let $N(t)$ stand in the place of divergences, rather than to try to use $1/t$ directly. The utility of this procedure is discussed in detail in a later section on numerical methods.

The first order of business is to provide an explicit expression for the divergent term. We can do this by considering a related and somewhat more interesting sum, the sum over second derivatives of z_n with respect to c. Realizing that each z_n is parameterized by c, we can take its derivative:

$$z'_{n+1} = \frac{d}{dc} z_{n+1} = 2 z'_n z_n + 1 \tag{9}$$

and

$$z''_{n+1} = \frac{d^2}{dc^2} z_{n+1} = 2\left(z''_n z_n + \left(z'_n\right)^2\right) \tag{10}$$

Figure 2: Divergent term

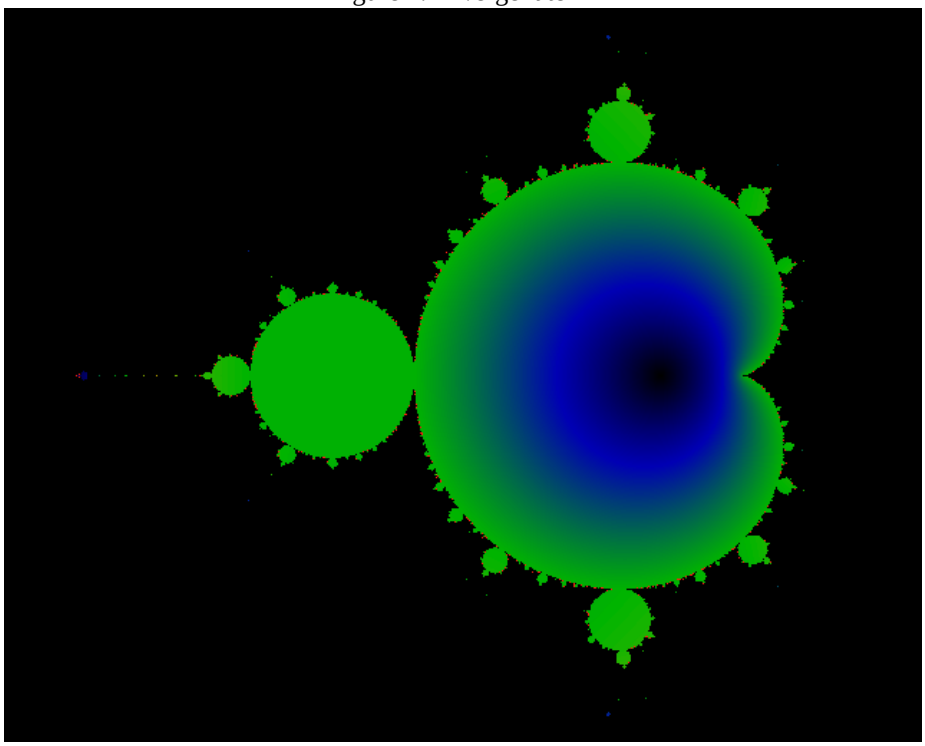

Plot of the divergent term of $S_c(t)$. The figure shows $\lim_{t->0^+} |S_c(t)|/N(t)$, where $|x+iy| = \sqrt{x^2+y^2}$ is the ordinary complex modulus. Black represents a value of zero, and green a value of 1/2. Points outside of the M-set are explicitly excluded from this picture. An explicit expression for this divergent term is given in the text.

Note that z_n, z'_n and z''_n are well defined for all values of c and finite n: they are entire functions, 'merely' polynomials in c. Note that these polynomials never involve $\bar{c}$, the complex conjugate of c, and thus all derivatives with respect to $\bar{c}$ are vanishing.

Let us then define the sum

$$P_c(t) = \sum_{n=0}^{\infty} z''_n \exp(-t^2 n^2) \tag{11}$$

Note that

$$P_c(t) = \frac{d^2}{dc^2} S_c(t) \tag{12}$$

holds for all positive t. $P_c(t)$ also diverges as $1/t$. Figures 3 and 4 shows the magnitude and phase of that divergence. By comparing the figures, it is relatively straightforward to determine that inside of the main cardiod, the divergent term of $P_c(t)$ is given by

$$P_c(t) = N(t) \; \frac{1}{4(\frac{1}{4} - c)^{3/2}} + o(1) \tag{13}$$

The divergent term term of $P_c(t)$ can be immediately integrated to obtain the divergent term in $S_c(t)$ inside the cardiod:

$$S_c(t) = N(t) \; \left[\frac{1}{2} - \sqrt{\frac{1}{4} - c} \right] + o(1) \tag{14}$$

If we write this divergent piece as $A(c) = \frac{1}{2} - \sqrt{\frac{1}{4} - c}$ then it is trivial to verify that $|A(c)| = 1/2$ on the boundary of the cardioid; that is, $\left|A(e^{i\phi}/2 - e^{2i\phi}/4)\right| = 1/2$ for all angles ϕ. The boundary of the cardioid is given by $x + iy = e^{i\phi}/2 - e^{2i\phi}/4$, of course. Next, we note that $A(c)$ represents a fixed-point of the Mandelbrot iterator: $A(c) = A^2(c) + c$. Indeed, this should not be a surprise: the divergent term of the sum $S_c(t)$ is in effect the average over over all values of z_n. Inside the main bulb, we have $\lim_{n\to\infty} z_n = A(c)$, and so of necessity, the leading divergence of the sum must be $A(c)$. Similarly, in the large bud on the left, z_n converges to a two-cycle, with $z_n \to -1/2 + i\sqrt{c + 3/4}$ and $z_{n+1} \to -1/2 - i\sqrt{c + 3/4}$. The average of these two values is $-1/2$, and so we can trivially deduce that $\lim_{t\to 0^+} S_c(t)/N(t) = -1/2$ and thus that $\lim_{t\to 0^+} |S_c(t)|/N(t) = 1/2$ which exactly matches our numerical results. In other buds, the sequence converges to m-cycles. Thus, in other buds, the divergent term will be the average over these m values of the limit cycle. Provided one can calculate this average, then one has an exact expression for the divergences of $S_c(t)$. Of course, there are considerable additional difficulties once one gets into the more contorted parts of the M-set, since the convergence to a limit cycle can be extremely slow, thus creating considerable topological difficulties when reasoning about the topology of the M-set and in particular, the validity of the expansion of terms in the formula 4. The remainder of this monograph concerns itself with the issue of the rate of convergence to the limit cycles, which we will find is given by the Dedekind eta.

Figure 3: Divergent Derivative

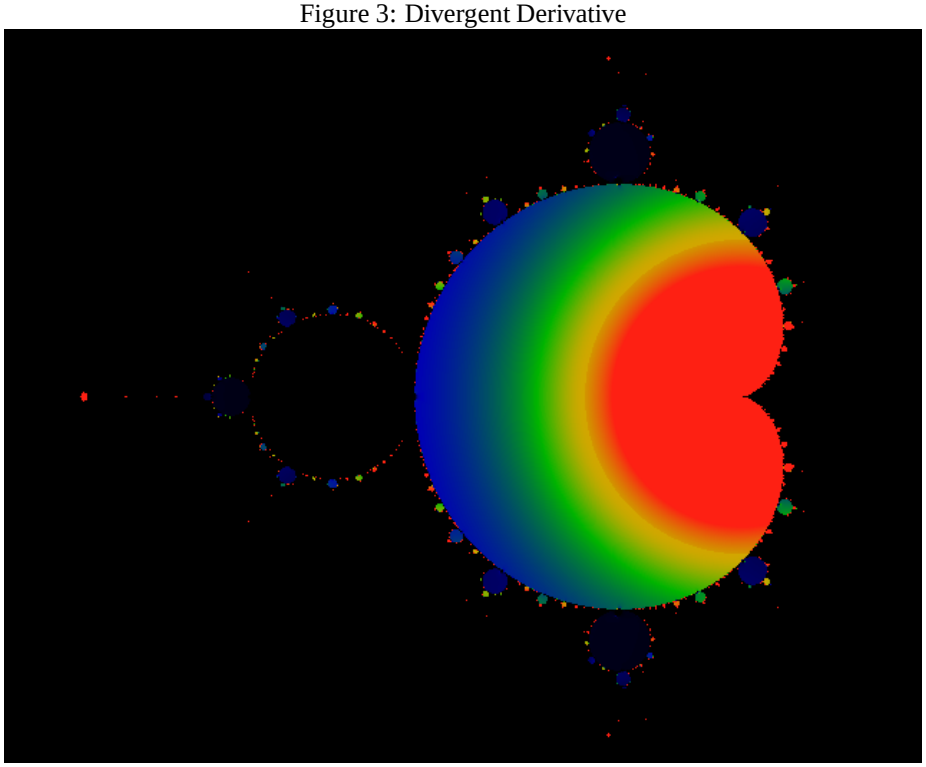

This picture shows the divergent term of $P_c(t)$, that is, $\lim_{t->0^+} |P_c(t)|/N(t)$. Red denotes any value equal or greater than 1, black corresponds to a value of zero. The value of this limit in the largest bud to the left is precisely zero over the entire bud. For the next smallest buds (at the top, bottom, and the second to the left), the value seems to be uniformly 1/30 across the whole bud, although there does seem to be a slight gradation which is hard to distinguish from numerical errors. By looking at this image, we can see that this limit seems to take on other, constant, values in the progressively smaller buds. The color scheme here has black <= 0.0, blue ~= 0.2, green ~= 0.5, yellow ~= 0.75, red >= 1.0. If the values were indeed constant over the smaller buds, this would have some interesting implications on the limit-cycles for these buds, as discussed in the text.

Figure 4: Divergent Phase

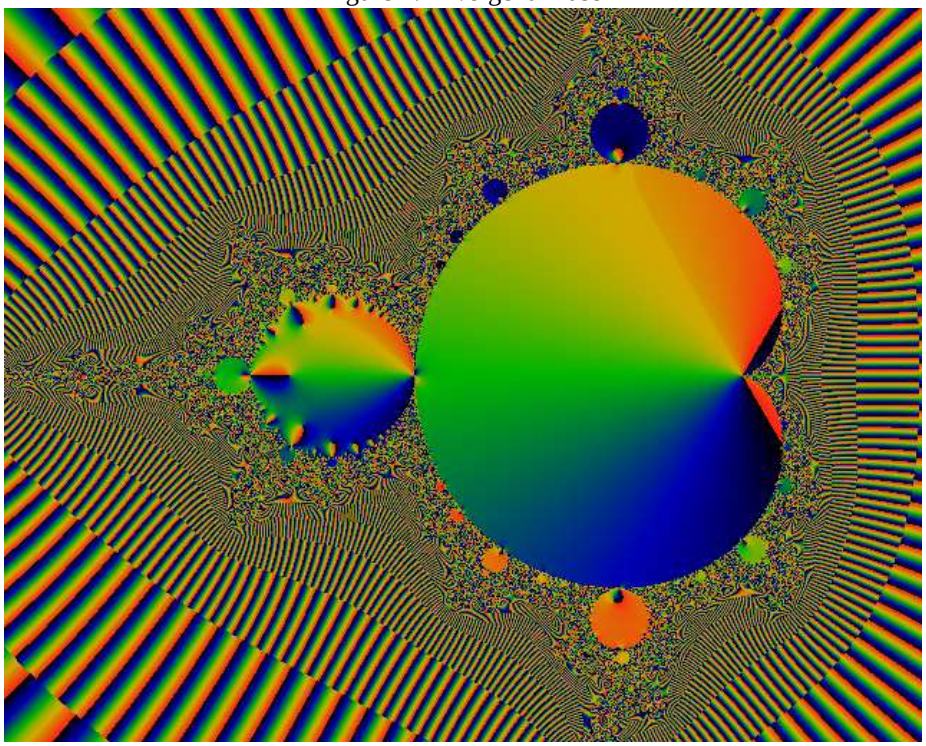

The phase of $P_c(t)$ in the limit of $t \to 0$. That is, it shows $\lim_{t\to 0^+} \arctan(\Im P_c(t)/\Re P_c(t))$. The color scheme is such that black=$-\pi$, green=0, red=$+\pi$. The rays on the outside of the set correspond to Duoady-Hubbard rays. Note the first hint of a modular form-like structure in the largest bulb immediately to the left of the main cardiod.

1.3 Finite Terms

Let us now turn to the finite remainders. By subtracting away the divergent pieces, we are essentially subtracting away the contribution of the asymptotic limit cycle. The remaining finite parts indicate how the asymptotic behavior is approached. If the finite part is large, this indicates that the iteration took a long time to approach the asymptotic limit. If the finite part is small, then the series converged to its limit cycle quickly. The figure 5 shows this rate of convergence. Curiously, we find that

$$\lim_{t\to 0^+} |S_c(t)| - N(t)\,|A(c)| + |S_c(t) - N(t)A(c)| \lesssim 0.01 \tag{15}$$

that is, the divergence of the modulus has the opposite sign from the divergence of the sum. This can only happen if the phase (the argument) of the finite part is opposite to the phase of $A(c)$. In other words,

$$\arg\left(S_c(t) - N(t)A(c)\right) \approx -\arg A(c) \tag{16}$$

The overall structure at first doesn't look all that inspiring. As before, we can discern considerably more structure if we examine $P_c(t)$ instead of $S_c(t)$. This reveals some of the true complexity in the system.

The finite term in the main cardiod is shown in figure 6 and at least a superficial resemblance to the image of the Dedekind zeta/Euler function shown in figure 1 should be immediately apparent.

It is important at this point to note that this last figure shows the modulus taken first, and then the divergence subtracted afterwards. This is not the same as subtracting the divergence first, and then taking the modulus. If we subtract the divergent complex term first, then we see in the main cardiod a figure that closely resembles that in figure 7, with a complex structure of poles located on the boundary, and zeros located inside.

1.4 The Circular Western Bud

The sums on the main circular bud immediately to the west of the cardioid do not have a divergent parts; the sums appear to be finite. The bud interior is shown in the figure 7.

The bud interior shows a remarkable visual resemblance to the divisor series

$$s_o(q) = \sum_{n=1}^{\infty} d(n)q^n = \sum_{n=1}^{\infty} \frac{q^n}{1-q^n} \tag{17}$$

constructed from the classic number-theoretic divisor function $d(n) = \sigma_0(n)$, the number of divisors of n. Figure 8 shows the divisor series.

Re-expressing the coordinates on the interior of the bud as

$$q = 4(c + 1.0) \tag{18}$$

so that the center of the bud occurs at $q = 0$ and the radius of the bud is $q = 1$, one can then produce a rough numeric fit to the q-series for the interior of the bud. It seems that

$$\lim_{t\to 0^+} P_c(t) = 3.0 + 7.5q + 10.8(3)\,q^2 + 19(2)\,q^3 + 0(1)\,q^4 + 13(30)\,q^5 + \ldots \tag{19}$$

Figure 5: Rate of Convergence

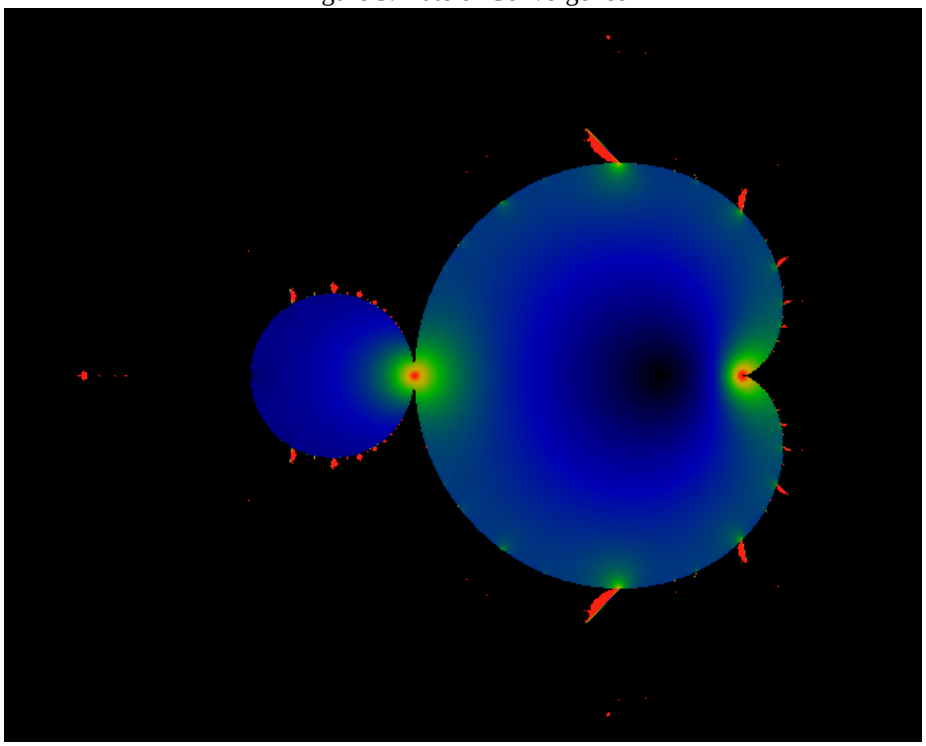

This figure shows the rate of convergence, that is, $\lim_{t\to 0^+} |S_c(t)| - N(t)\,|A(c)|$. We take $A(c)$ to be as given in the text for the main cardiod, and equal to precisely 1/2 in the largest bud. For this numerical calculation, we take it to be zero everywhere else, thus leading to artifacts outside the main cardiod and bulb, where in fact $A(c)$ shouldn't be zero. The color ramp has been scaled by -1: i.e. black = 0, green ~= -0.5, red <= -1.0. There appear to be a number of poles arrayed along the perimeter of the cardiod, located at the tangent points of the bulbs. The pole at the unicorn horn and at the largest bulb is clearly visible. These poles indicate areas where the iterated series has a very difficult time converging to a limit cycle. There is considerably more structure inside of this image than is immediately evident. The structure is exhibited when one examines the non-divergent parts of $P_c(t)$ instead.

Figure 6: Mandelbrot Interior

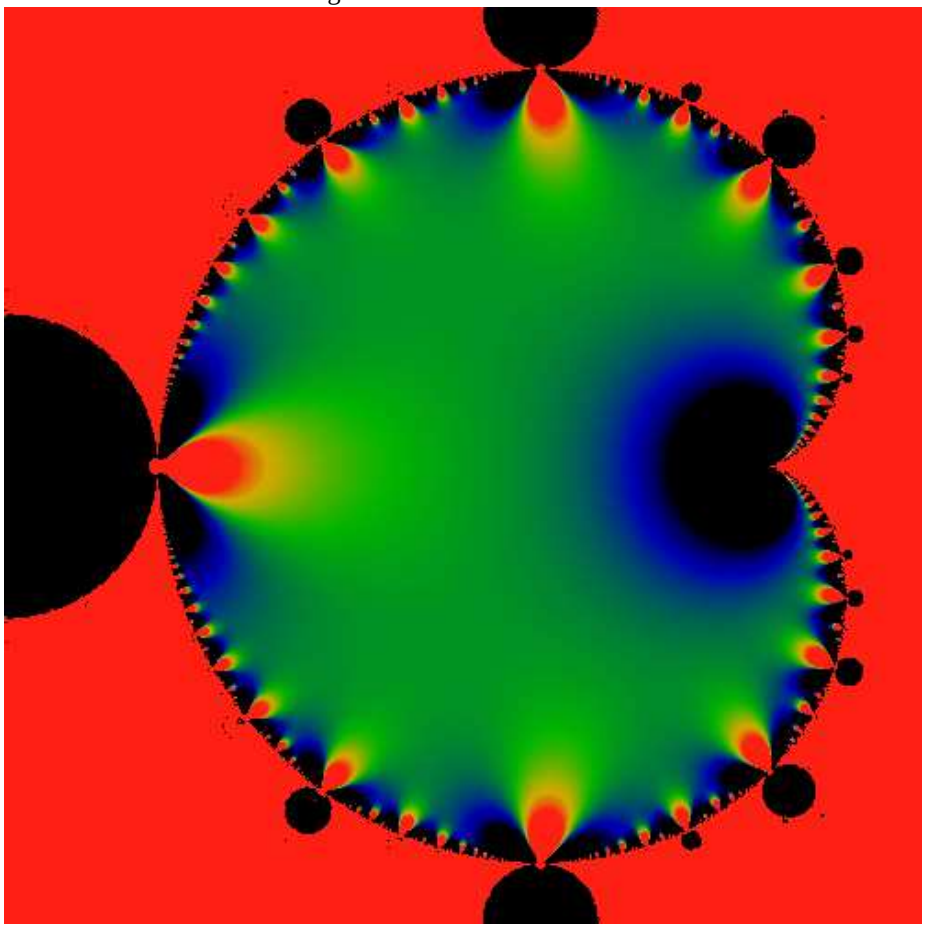

The image above shows the finite piece in the main bulb, after the divergent piece has been subtracted. That is, it shows $\lim_{t\to 0} |P_c(t)| - N(t)\left|(1/4-c)^{-3/2}/4\right|$. It appears to have dipoles (saddles) arrayed along the perimeter. There don't seem to be any simple zeros. The color scheme has been adjusted so that black <= -10, green ~= 0 and red >= 10. These (multi-)poles visually indicate something that is commonly known: the series has a hard time converging near the tips of the horns.

Figure 7: Bud Interior

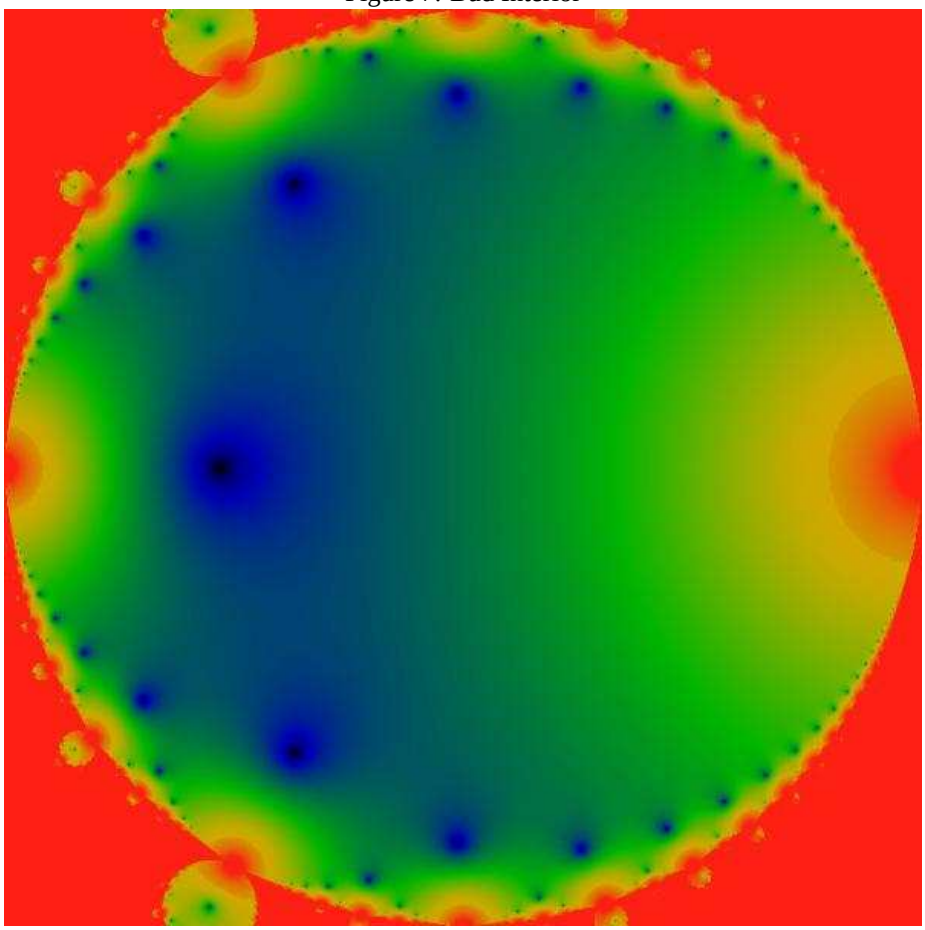

The sum $P_c(t)$ doesn't have a divergent piece in the large bud. This image shows $\lim_{t\to 0^+} |P_c(t)|$ for the square area $\Re c \in [-1.25, -0.75]$. As can be seen, there is a considerable amount of structure here. There seem to be poles located on the boundary, where-ever another bud is tangent to this one. This is of course everywhere, since a bud is tangent for every possible rational angle. The strength of the pole is somehow proportionate to the size of the bud; the residue of the poles all seem to be the same sign. Note there seems to be a sequences of zeros inside the bud. The color ramp has been logarithmically compressed to highlight the zeros: black = 0, green ~= 10, red >= 100.

A very similar figure results if one graphs the finite part on the main cardiod, after removing the divergence. That is, the graph for $\lim_{t\to 0} \left|P_c(t) - N(t)(1/4-c)^{-3/2}/4\right|$ in the main cardiod is essentially the same.

Figure 8: Divisor Series on the q-disk

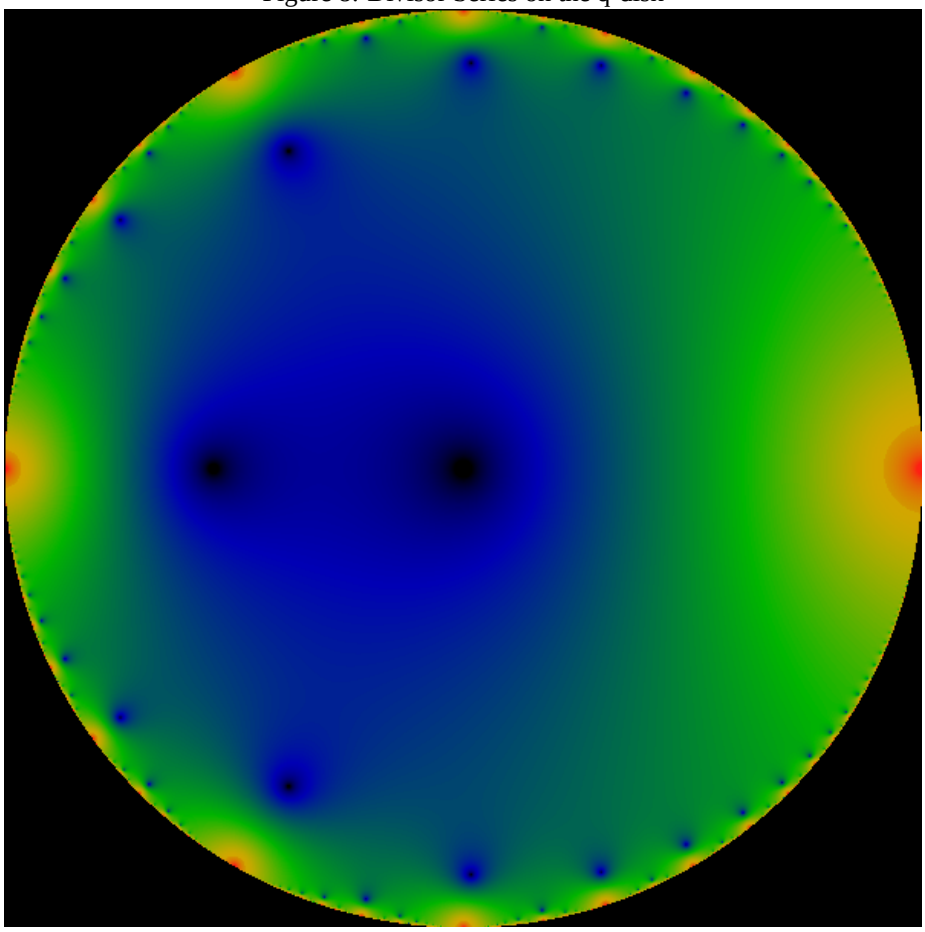

The sum $|\sum_{n=1}^{\infty} q^n/(1-q^n)|$ on the unit disk. The colormap is logarithmically compressed, so that blue represents ares with a value of less than one, and green represents areas with a value of more than 10.

The numbers in parenthesis give the uncertainty in the least significant digit. This is a fairly quick and rough fit; only the values of the first two terms seem certain, and that the coefficient of q^4 seems to vanish.

1.5 Mobius Transformations on the Disk

Figure 9 shows the real part of $P_c(0)$ in the bud.

Explicit numerical work shows that it does not seem to be a modular form of integer weight. Nor does it seem to be a modular form of fractional weight. But it sure seems to "come close". Lets review what this means.

Modular symmetry on the q-disk is best explored by mapping the q-disk to the Poincare upper half-plane, applying a Mobius transformation there, and then mapping back. Given a point τin the upper half-plane, i.e. $\Im\tau > 0$, one maps to the q-disk with

$$q = e^{2i\pi\tau} \tag{20}$$

One can then apply a Mobius transform to τ on the upper half plane:

$$\tau \to \frac{a\tau + b}{c\tau + d} \tag{21}$$

and then map this back to the q-disk coordinates.

A function f on the upper half-plane is said to be a *modular form* if

$$f\left(\frac{a\tau + b}{c\tau + d}\right) = (c\tau + d)^k f(\tau) \tag{22}$$

for integers a, b, c, d satisfying $ad - bc = 1$. The constant k is said to be the *weight* of the form. Mapped to the upper half-plane, the interior of the bud does not seem to be a modular form for any real value of k. In particular, equation22 doesn't quite seem to hold even if the absolute value of each side is taken, although it seems to "come close" in certain situations.

1.6 Self-Similarity on the Poincare Disk

There is one interesting mapping whose properties are worth reviewing, and that is the mapping of the upper half-plane to the Poincare disk. This mapping is curious because it is not infrequent in the literature, and because a periodic function on the upper half-plane takes the appearance of a self-similar function on the disk.

The mapping if the upper half-plane to the Poincare disk is given by

$$w = \frac{i - \tau}{i + \tau} \tag{23}$$

This map is a conformal map that takes points in the upper half-plane to points in the interior of a unit disk. Points on the real number line (points with a zero imaginary component) are mapped to the edge of the disk. Let $\tau = x + i\varepsilon$ and take $\varepsilon \to 0$; one then has

$$w = \frac{i - x}{i + x} = \frac{x^2 - 1 + 2ix}{x^2 + 1} \tag{24}$$

Figure 9: Real Part

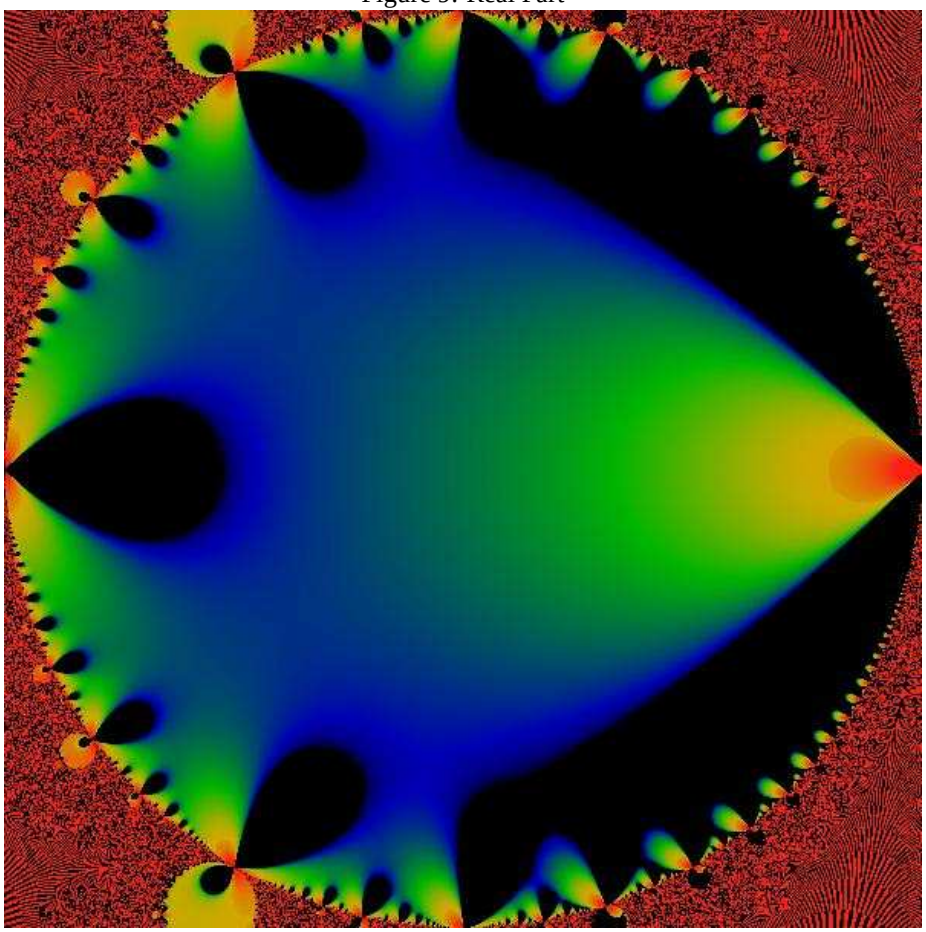

This figure shows the real part of $\lim_{t\to 0^+} P_c(t)$ in the western bud. The color scheme is identical to that used to show the modulus. Black areas here represent negative values for the real part. A similar graph of the divisor series would have more or less a rather similar look.

It is not hard to show that $|w| = 1$; that is w is on the edge of the disk. A function which is periodic in τ with integer periodicity will manifest itself with an M-set like periodicity on the circumference of the Poincare disk. Specifically, a feature located at integer values of $x = n$ will have a specific angular location on the Poincare disk, which is obtained by solving for the angle θ in

$$w_n = \cos\theta_n + i\sin\theta_n = \frac{n^2-1}{n^2+1} + i\frac{2n}{n^2+1} \tag{25}$$

In particular, the region $n \leq \Re\tau \leq n+1$ is mapped to the angular interval $[\theta_n, \theta_{n+1}]$.

Images constructed by mapping the q-disk to upper half-plane, via equation 20, will be inherently periodic. The Mobius transform

$$\tau \to \tau + m \tag{26}$$

under the q-disk mapping takes all such values to exactly the same value of q. An image on the Poincare disk constructed from the image on the q-disk will have regions that are identical, by construction.

The figures 10 and 11 show a mapping of the western bud to the Poincare disk. More precisely, the mapping is actually a half-angle mapping, taking q to $\exp i\pi\tau$ instead of $\exp 2i\pi\tau$, and then re-mapping to the Poincare disk. The result of the half-angle mapping is that the figures do not have the left-right symmetry $\tau \to -1/\tau$, but this is only an artifact of the construction.

1.7 Re-mapping the Cardioid

In order to proceed with the exploration of the interior of the Mandelbrot set as a modular form, we need to find a way of mapping the the cardioid to the complex upper half-plane. The most obvious mapping is to express the interior in terms of the coordinates ρ and ϕ with the interior given by

$$c = \left(\frac{\rho e^{i\phi}}{2}\right)^2 - \frac{\rho e^{i\phi}}{2} \tag{27}$$

Thus, the rectangle $0 \leq \rho \leq 1$ and $-\pi \leq \phi \leq \pi$is mapped to the interior of the cardioid. The result of this mapping is shown in figure12.

The linearized coordinates can be immediately remapped to a circle by using the coordinates

$$q = \rho e^{i\phi + i\pi} \tag{28}$$

where an extra factor of -1 is introduced to left-right reverse the image. This extra flip is needed to bring the coordinate system precisely into line with the Poincare punctured disk coordinates. The punctured disk coordinates are sometimes referred to as the "nome" coordinates of elliptic geometry. These are defined as follows. Let $\tau = \omega_2/\omega_1$ be the so-called "half-period ratio", where ω_1 and ω_2 are the periods of an elliptic function, such as the Weierstrass $\wp$function. Then τ is a coordinate on the upper half-plane, with $\Im\tau > 0$. The traditional "fundamental region" on the upper half-plane is

Figure 10: Poincare Disk

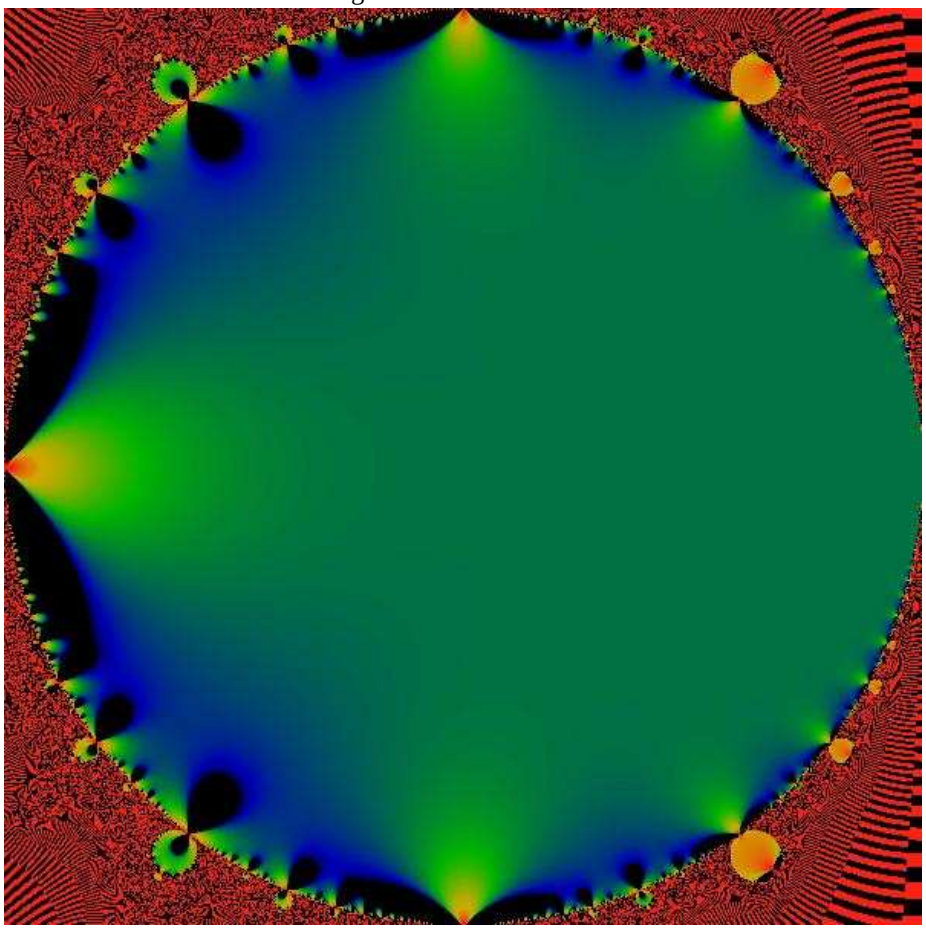

This figure shows the real part of $\lim_{t\to 0^+} P_c(t)$ in the western bud, remapped onto the Poincare disk by the half-angle mapping. To be precise, one maps the bud coordinates to q by equation 18, then maps $q = \exp i\pi\tau$, and finally uses equation 23 to map to the disk. The color scheme is identical to that used in other graphs.

Figure 11: Imaginary Part on Poincare Disk

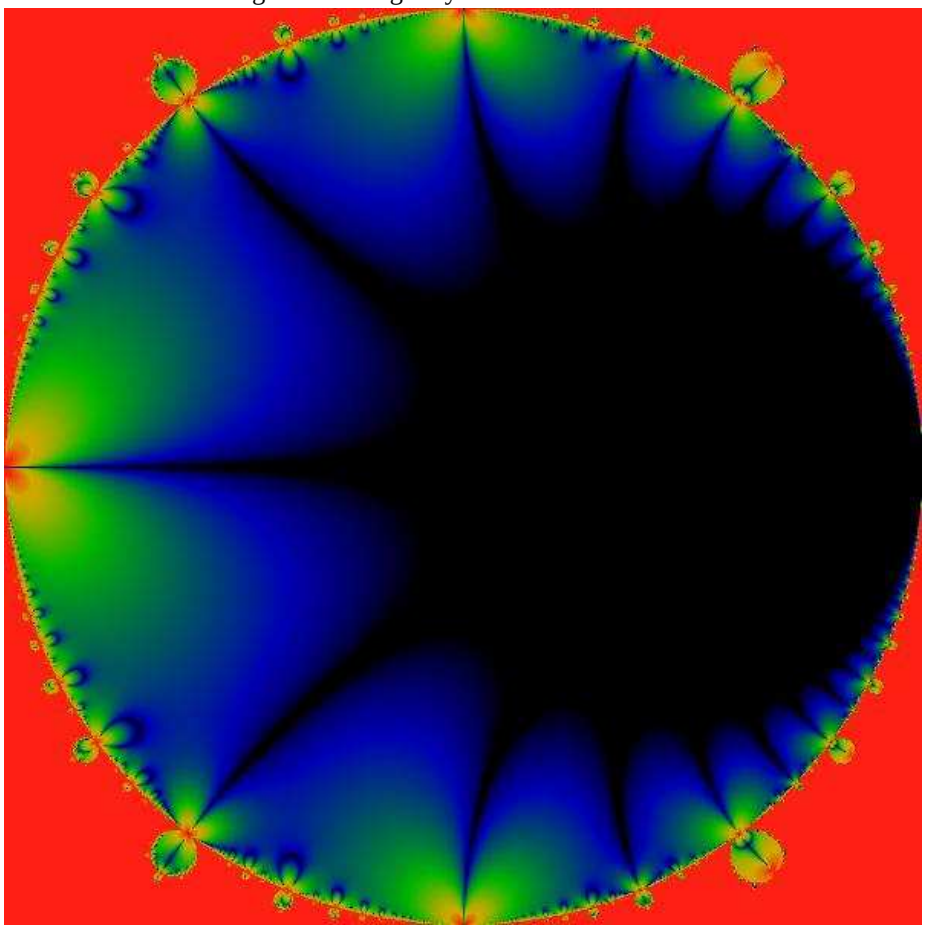

This figure shows the absolute value of the imaginary part of $\lim_{t\to 0^+} P_c(t)$ in the western bud, remapped by means of the half-angle mapping, onto the Poincare disk. The color scheme is identical to that used in other graphs. As the values shown here are by definition positive, the color black corresponds to small but positive values.

Figure 12: Linearized Cardioid

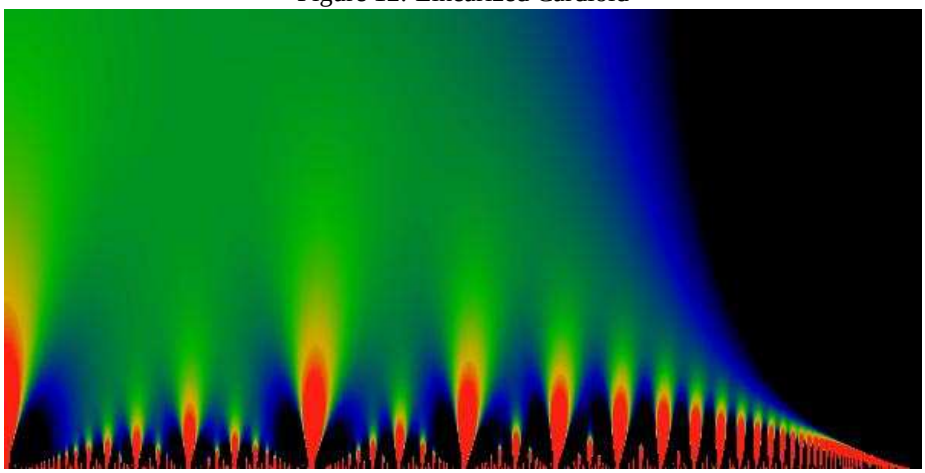

The Mandelbrot cardioid interior, using the coordinates of equation 27, for the range $0 \leq \rho \leq 1$ and $0 \leq \phi \leq \pi$. Note that each of the "flames" in this picture lean ever so slightly over to the right, rather than being completely vertical. The color scheme used is identical to that of the figure 6.

defined as the region $-1/2 < \Re\tau \leq 1/2$ and $|\tau| > 1$. This coordinate system on the upper half-plane can be mapped to the punctured disk as

$$q = e^{i\pi\tau} \tag{29}$$

with the word "puncture" referring to the fact that $q = 0$ never occurs for finite values of τ. This mapping maps the upper half-plane to values of $|q| < 1$. The orientation of this mapping is specifically picked in order to be consistent with standard definitions of modular functions on the punctured disk. For example, the Euler phi-function, expressed in q coordinates, is

$$\phi(q) = \prod_{k=1}^{\infty}(1-q^k) \tag{30}$$

and is show in figure 1.

The cardioid interior should be compared to the image of the Weierstrass invariant g_2, shown in figure 14.

By comparing the figures for the interior of the Mandelbrot set and the Weierstrass elliptic invariant, a general resemblance becomes painfully apparent, even if not explicitly demonstrated.

By construction, the function just demonstrated on the interior of the Mandelbrot set is a real function. To more fully explore the modular symmetry, we really need a complex function, that is, one with real and imaginary parts. Such a function is provided by not working with the modulus, but subtracting the divergence directly; this is explored in the next section.

Figure 13: Circularized Cardioid

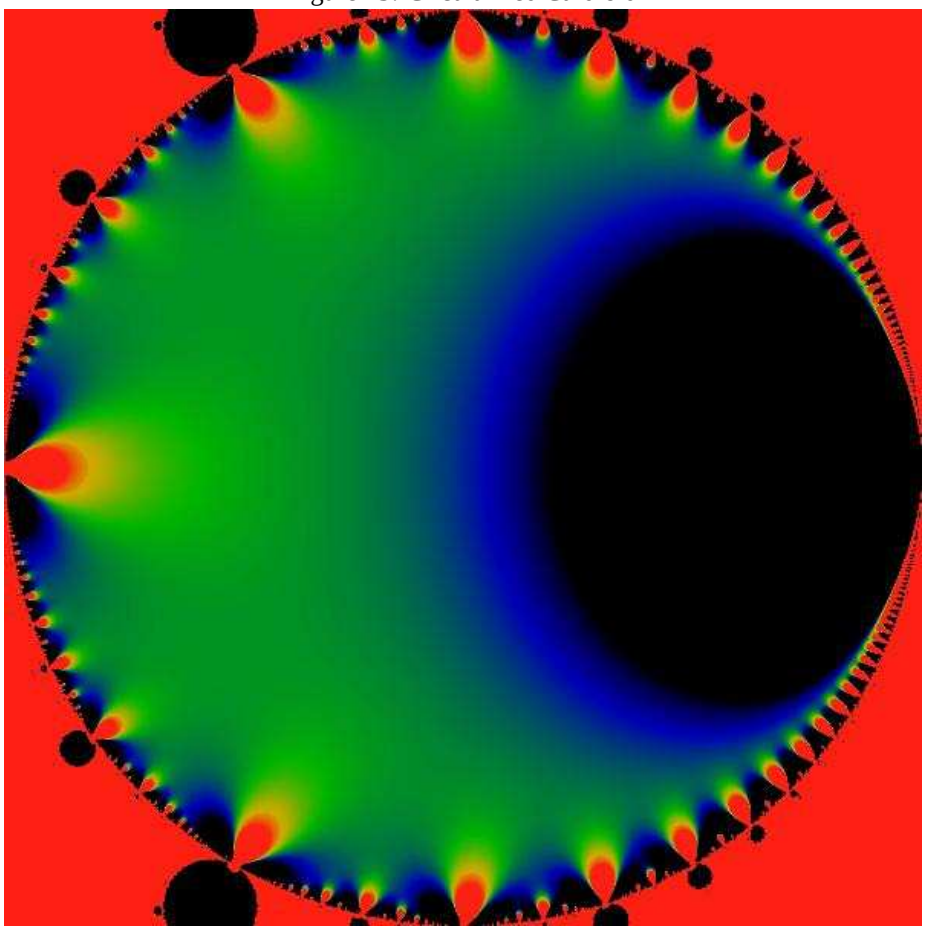

The cardioid interior remapped to the circle $\rho e^{i\phi+i\pi}$. Bulbs on the exterior of the Mandelbrot set are also visible in this remapping. The color scheme used is identical to that of the figure 6. The additional factor of $e^{i\pi}$ merely left-right reflects the image.

Figure 14: Weierstrass invariant

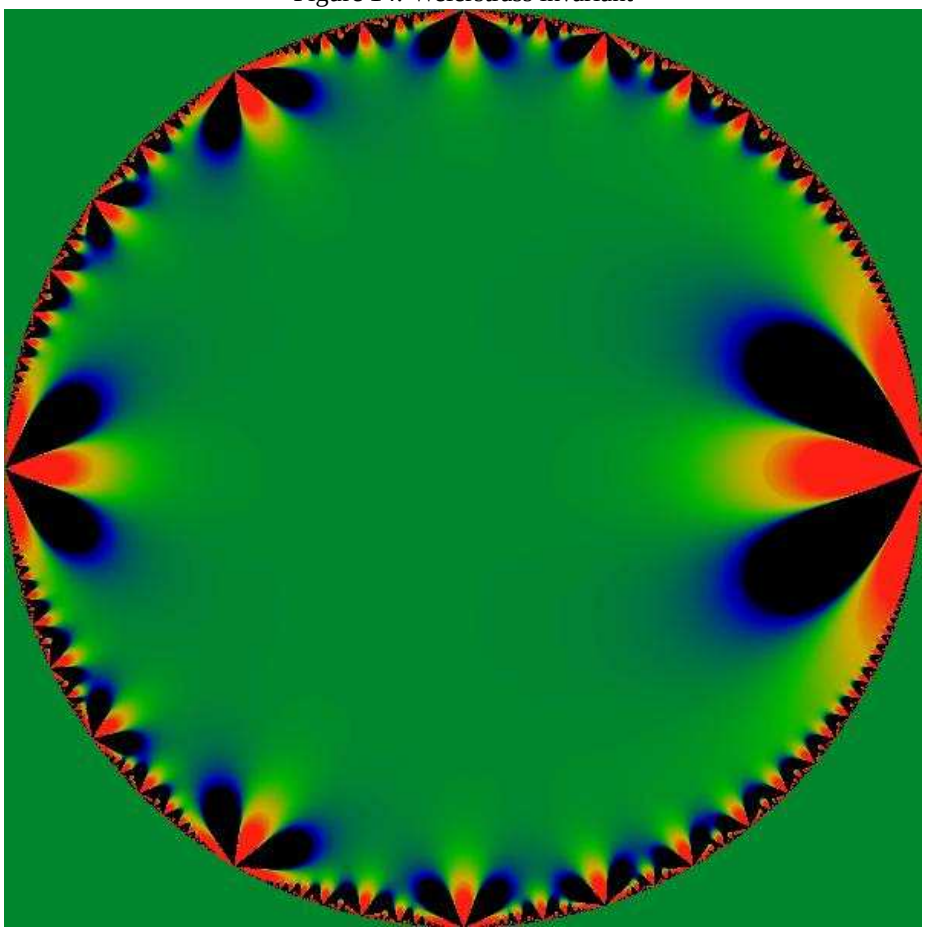

An image of the the real part of the Weierstrass invariant g_2 expressed in q coordinates. This function can be written explicitly as

$$g_2(\tau) = \frac{4\pi^4}{3}\left[1 + 240\sum_{k=1}^{\infty}\sigma_3(k)q^{2k}\right]$$

which can be re-expressed as a Lambert series

$$g_2(\tau) = \frac{4\pi^4}{3}\left[1 + 240\sum_{k=1}^{\infty}\frac{k^3 q^{2k}}{1-q^{2k}}\right]$$

This image uses a highly compressed logarithmic color scale adjusted to resemble that used for the Mandelbrot interior. Note that the modulus of $g_2$does not show this lobe structure; the real and imaginary parts of this function have complementary values. Graphs of g_3 resemble this figure, as do those of higher terms in the Eisenstein series. As one goes up the series, the number of lobes increases arithmetically. For example, the above figure shows three red lobes; the comparable figure for g_3 shows four lobes.

There is also a more subtle issue. It is not clear that the simple cardiod mapping 27 is the correct mapping. If one examines the figures, one can note a subtle, ever-so-slightly visible feature. Each of the "flames" in the figure lean slightly over to the right. Under Mobius transforms, this tilt is preserved, destroying the naive symmetry. Its possible that the mapping from cardioid to q coordinates is not the right mapping, and that some other, more complex mapping is required. What this mapping may be is not clear at this point.

This problem is presumably related to the fact that the buds on the exterior of the M-set are almost circles, but not quite (with the exception of the main bud to the west). If one could find a suitable remapping on the exterior, that mapping might presumably carry over into the interior as well, and vice-versa.

1.8 The Finite Part in the Cardioid

Lets revisit, this time exploring the function

$$\Xi(c) = \lim_{t\to 0} \left[P_c(t) - N(t) \, \frac{\left(\frac{1}{4} - c\right)^{3/2}}{4} \right] \tag{31}$$

Using the mappings given previously, $\Xi(c)$ can be re-expressed as $\Xi(q)$ on the q-disk. It is shown in the figures 15 and 16 and 17.

Despite the remarkably suggestive graphics, it seems that Ξ is not a modular form either; in particular, I was unable to find a real-valued number k for which even the less-demanding relation

$$\left| \Xi\left(\frac{a\tau + b}{c\tau + d}\right) \right| = \left| (c\tau + d)^k \Xi(\tau) \right| \tag{32}$$

held true. (Here, the use of the symbol τimplies that the relation was search for on the upper half-plane and not on the disk). It certainly remains quite possible that Ξ minus some constant will be a modular form, or that some further transformation of Ξ will render it so.

1.9 Appendix: Numeric Techniques

This section reviews the numeric techniques applied to perform the series sums. Specifically, some well-known techniques for series acceleration are applied; but these are not so well known as not to merit review.

Note that the series explored on these pages can be slow to converge, especially near the 'horns' of the Mandelbrot set. There are several well-known and established techniques of series acceleration that can improve the convergence. This section quickly reviews the technique used in this paper.

Consider the sum

$$A(t) = \sum_{n=0}^{\infty} a_n \exp(-t^2 n^2) \tag{33}$$

Assume that this sum converges in the limit of $t \to 0^+$, but possibly slowly. One can get a much more quickly-converging series by computing, in addition to $A(t)$, the

Figure 15: Cardioid Finite Part

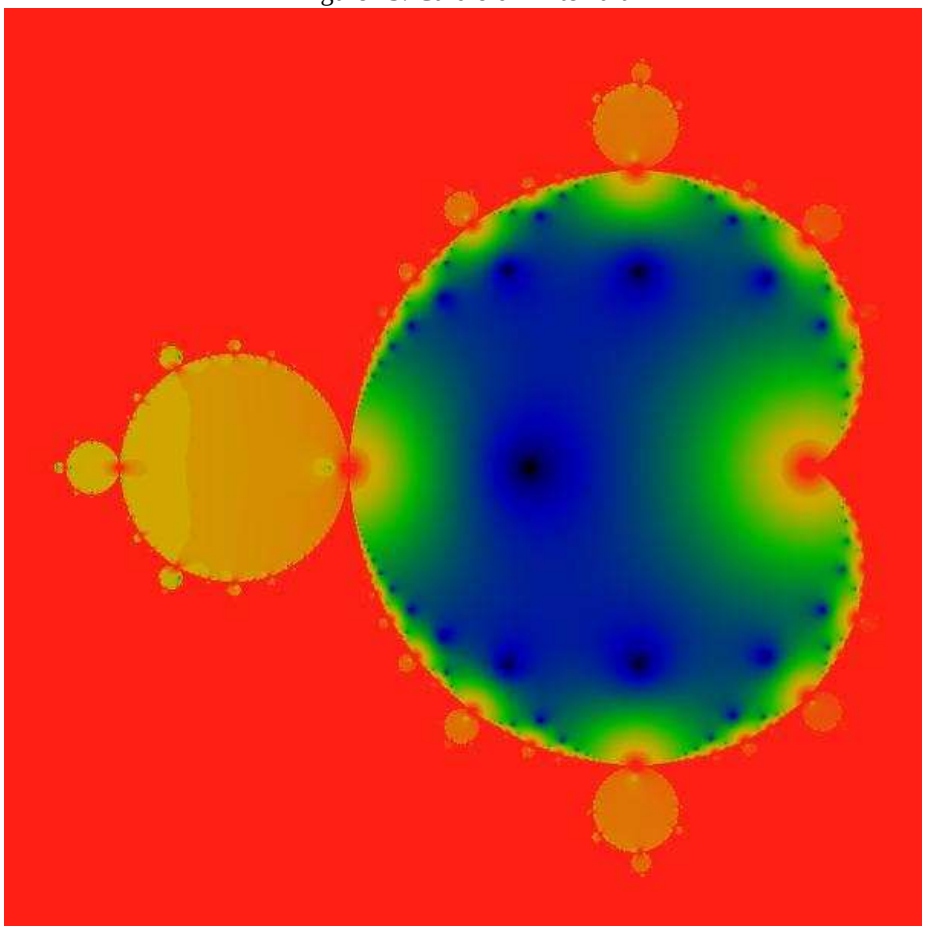

This figure shows the modulus of the finite part $|\Xi(c)|$. Some of the rest of the M-set is visible, but for the most part is blanked out by the subtraction of the divergent term in the main cardioid. Since this divergent term is inappropriate for the other parts of the M-set, these other features wash out. The same compressed logarithmic color scheme is used as in the other illustrations.

Figure 16: Cardioid Remapped

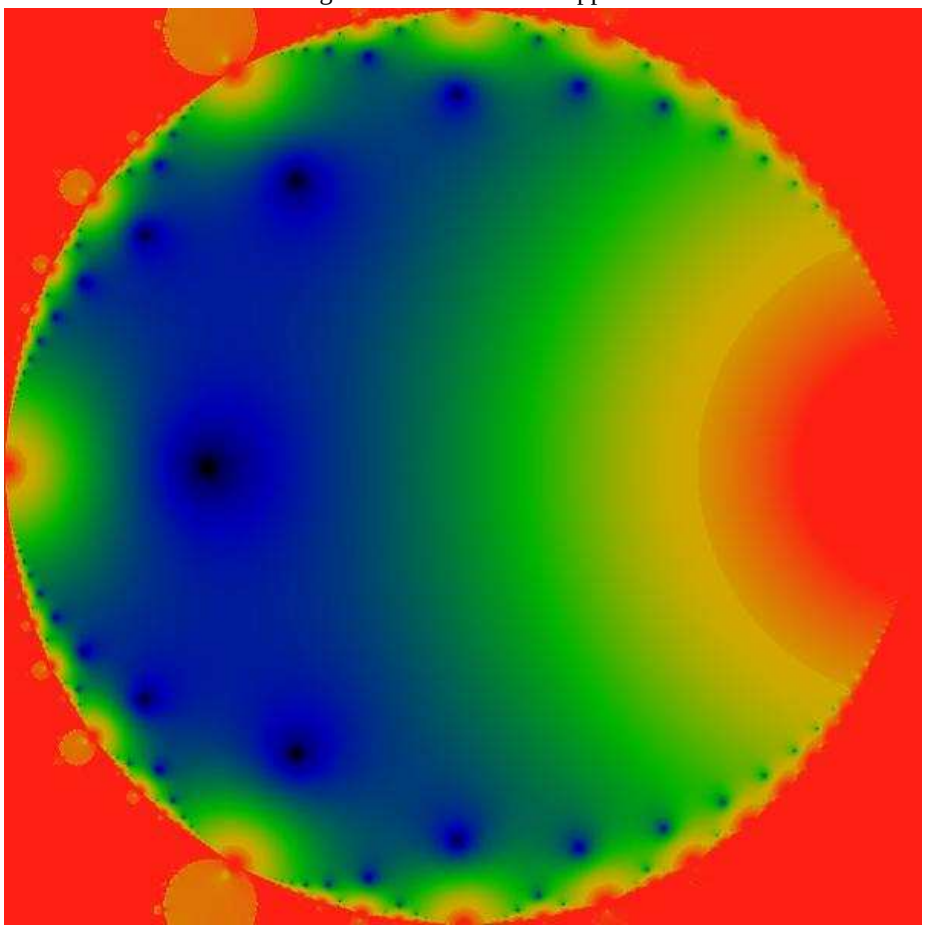

The finite part $|\Xi(q)|$, that is, $|\Xi(c)|$ remapped to the q-disk. The color scheme is the same as in the other images. Note the resemblance to the figure 7, but note that there are also differences between these figures. In particular, the divergence on the right hand side of this figure is stronger.

Figure 17: Finite Real Part

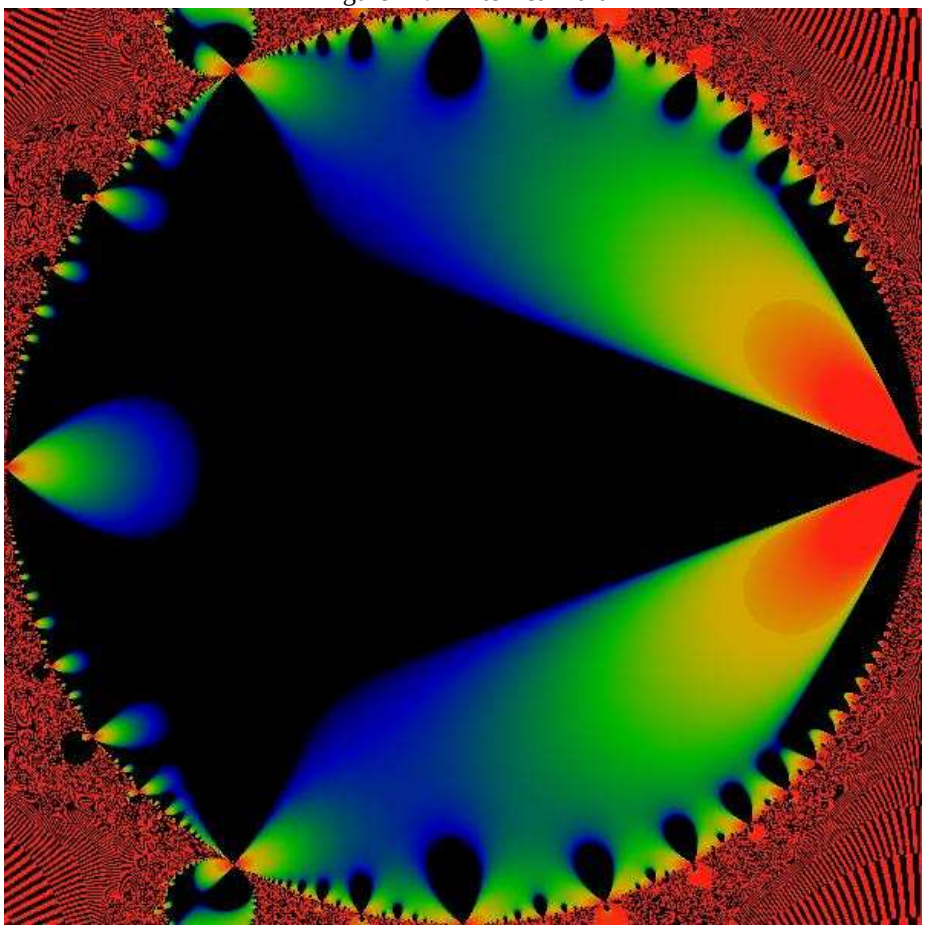

The real part $\Re\Xi(q)$ on the q-disk. The same color scheme is used as elsewhere.

derivatives $dA(t)/dt$ and $d^2A(t)/dt^2$. One then recombines these derivatives to form the quantity

$$B(t) = A(t) - t\frac{d}{dt}A(t) - \frac{t^2}{2}\frac{d^2}{dt^2}A(t) \tag{34}$$

It is clear that if the limit $A(0)$ exists and is finite, then one has

$$\lim_{t\to 0+} B(t) = \lim_{t\to 0+} A(t) \tag{35}$$

and furthermore, for small t, one has

$$B(t) = A(0) + o\left(t^3\right) \tag{36}$$

The correctness of equation 36 at first seems naively 'obvious' but is in fact quite subtle, and depends on having a series $\{a_n\}$ that is 'well-behaved' in certain ways.

The study of such series and the numerical techniques to sum them falls under the name of 'series acceleration' and is a well-developed branch of mathematics in its own right. It is outside of the scope of this section to review any deeper results. Suffice it to say that this entire paper is predicated on the assumption that the equation 36 does hold for the sums encountered. This does seem to be the case, but is hardly obvious from first principles, especially for points in troublesome sections of the M-set. By contrast, in the well-behaved areas of the M-set, it is straightforward to verify that equation 36 holds, and that the resulting sums are accurate for five to ten decimal places, corresponding to t values in the range of 0.01 to 0.001 for sums with 2 to 50 thousand terms.

Some of the sums in encountered in this paper are divergent. The simplest such sums have a limit point, namely

$$\lim_{n\to\infty} a_n = \text{const.} \neq 0 \tag{37}$$

in which case one has

$$A(t) = \frac{\text{const.}}{t}\sqrt{\frac{\pi}{4}} + o\left(1\right) \tag{38}$$

The extra factor of $\sqrt{\pi}/2$ comes from the behavior of the Gaussian regulator; that is,

$$N(t) = \sum_{n=0}^{\infty} \exp(-t^2n^2) = \frac{1}{t}\sqrt{\frac{\pi}{4}} + o\left(1\right) \tag{39}$$

In order to correctly subtract this linear divergence from a divergent sum, one is advised to subtract $N(t)$ rather than $1/t$ directly. This advice comes from the need to subtract the divergence so that the equation 36 is not violated. In general, $N(t)$ will have $o\left(1\right)$, $o\left(t\right)$ and $o\left(t^2\right)$ terms as well, any one of which will mess up equation 36 if not properly accounted for. Thus, in general, the correct way to subtract a divergent term is to form

$$A'(t) = A(t) - \text{const. } N(t) \tag{40}$$

and then form $B'(t)$ from $A'(t)$ to obtain the finite part. One can perform the subtraction 40 under the summation, or outside of it. Performing it under the summation potentially

minimizes round-off errors. Note that these considerations apply to series with limit cycles as well as limit points. That is, the a_n need not converge to a point; as long as they do converge to a limit cycle, this mechanism of subtracting the divergent piece will work.

One final remark: note that, in general, after removing a linear divergence in a summation, the next leading order need not be finite, but may be a weaker divergence, such as a logarithmic divergence. This is presumably the nature of the divergences seen at the horns of the M-set, for example. On the complex plane, finite sums grow until they hit a pole. At the pole, the sums are logarithmically divergent.

1.10 Summary

This paper reprises and revises an earlier draft from November 2000, located at `http://www.linas.org/art-gallery/spectral/spectral.html`.

Although an explicit expression for the apparent modular symmetry was not found, it is believed that a convincing argument has been made that such a symmetry lurks within the asymptotic limits of the Mandelbrot iterator. Specifically, the actual symmetry appears to most closely resemble that of sums involving the number-theoretic divisor function. Obtaining an explicit form will open up additional avenues of research, possibly shedding light on the maddening contour of the Mandelbrot Set.

What more can we say? This is wild stuff.

References

[Apo90] Tom M. Apostol, *Modular Functions and Dirichlet Series in Number Theory*, Springer Verlag, New York, 1990.

[WMF] Wikipedia, *Modular forms*, `http://en.wikipedia.org/wiki/Modular_form`

[Lin00] Linas Vepstas, *Spectral Analysis of Mandelbrot Interior*, (2000) located at `http://www.linas.org/art-gallery/spectral/spectral.html`.